


**Observation of the decay  $B^0 \rightarrow J/\psi\omega$  at Belle II**

I. Adachi<sup>1</sup>, L. Aggarwal<sup>2</sup>, H. Ahmed<sup>3</sup>, H. Aihara<sup>4</sup>, N. Akopov<sup>5</sup>, M. Alhakami<sup>6</sup>, A. Aloisio<sup>7</sup>, N. Althubiti<sup>8</sup>, N. Anh Ky<sup>9</sup>, D. M. Asner<sup>10</sup>, H. Atmacan<sup>11</sup>, V. Aushev<sup>12</sup>, M. Aversano<sup>13</sup>, R. Ayad<sup>14</sup>, V. Babu<sup>15</sup>, N. K. Baghel<sup>16</sup>, S. Bahinipati<sup>17</sup>, P. Bambade<sup>18</sup>, Sw. Banerjee<sup>19</sup>, M. Barrett<sup>20</sup>, J. Baudot<sup>21</sup>, A. Baur<sup>22</sup>, A. Beaubien<sup>23</sup>, J. Becker<sup>24</sup>, J. V. Bennett<sup>25</sup>, V. Bertacchi<sup>26</sup>, M. Bertemes<sup>27</sup>, E. Bertholet<sup>28</sup>, M. Bessner<sup>29</sup>, S. Bettarini<sup>30</sup>, B. Bhuyan<sup>31</sup>, F. Bianchi<sup>32</sup>, D. Biswas<sup>33</sup>, A. Bobrov<sup>34</sup>, D. Bodrov<sup>35</sup>, A. Bolz<sup>36</sup>, A. Bondar<sup>37</sup>, J. Borah<sup>38</sup>, A. Boschetti<sup>39</sup>, A. Bozek<sup>40</sup>, M. Bračko<sup>41</sup>, P. Branchini<sup>42</sup>, N. Brenny<sup>43</sup>, R. A. Briere<sup>44</sup>, T. E. Browder<sup>45</sup>, A. Budano<sup>46</sup>, S. Bussino<sup>47</sup>, Q. Campagna<sup>48</sup>, M. Campajola<sup>49</sup>, G. Casarosa<sup>50</sup>, C. Cecchi<sup>51</sup>, J. Cerasoli<sup>52</sup>, M.-C. Chang<sup>53</sup>, R. Cheaib<sup>54</sup>, P. Cheema<sup>55</sup>, C. Chen<sup>56</sup>, B. G. Cheon<sup>57</sup>, K. Chilikin<sup>58</sup>, K. Chirapatpimol<sup>59</sup>, H.-E. Cho<sup>60</sup>, K. Cho<sup>61</sup>, S.-J. Cho<sup>62</sup>, S.-K. Choi<sup>63</sup>, S. Choudhury<sup>64</sup>, J. Cochran<sup>65</sup>, L. Corona<sup>66</sup>, J. X. Cui<sup>67</sup>, E. De La Cruz-Burelo<sup>68</sup>, S. A. De La Motte<sup>69</sup>, G. de Marino<sup>70</sup>, G. De Nardo<sup>71</sup>, G. De Pietro<sup>72</sup>, R. de Sangro<sup>73</sup>, M. Destefanis<sup>74</sup>, S. Dey<sup>75</sup>, A. Di Canto<sup>76</sup>, F. Di Capua<sup>77</sup>, J. Dingfelder<sup>78</sup>, Z. Doležal<sup>79</sup>, I. Domínguez Jiménez<sup>80</sup>, T. V. Dong<sup>81</sup>, X. Dong<sup>82</sup>, M. Dorigo<sup>83</sup>, D. Dossett<sup>84</sup>, K. Dugic<sup>85</sup>, G. Dujany<sup>86</sup>, P. Ecker<sup>87</sup>, D. Epifanov<sup>88</sup>, J. Eppelt<sup>89</sup>, P. Feichtinger<sup>90</sup>, T. Ferber<sup>91</sup>, T. Fillinger<sup>92</sup>, C. Finck<sup>93</sup>, G. Finocchiaro<sup>94</sup>, A. Fodor<sup>95</sup>, F. Forti<sup>96</sup>, B. G. Fulsom<sup>97</sup>, A. Gabrielli<sup>98</sup>, E. Ganiev<sup>99</sup>, M. Garcia-Hernandez<sup>100</sup>, G. Gaudino<sup>101</sup>, V. Gaur<sup>102</sup>, A. Gaz<sup>103</sup>, A. Gellrich<sup>104</sup>, G. Ghevondyan<sup>105</sup>, D. Ghosh<sup>106</sup>, H. Ghumaryan<sup>107</sup>, G. Giakoustidis<sup>108</sup>, R. Giordano<sup>109</sup>, A. Giri<sup>110</sup>, P. Gironella Gironell<sup>111</sup>, A. Glazov<sup>112</sup>, B. Gobbo<sup>113</sup>, R. Godang<sup>114</sup>, O. Gogota<sup>115</sup>, P. Goldenzweig<sup>116</sup>, W. Gradl<sup>117</sup>, E. Graziani<sup>118</sup>, D. Greenwald<sup>119</sup>, Z. Gruberová<sup>120</sup>, Y. Guan<sup>121</sup>, K. Gudkova<sup>122</sup>, I. Haide<sup>123</sup>, C. Harris<sup>124</sup>, K. Hayasaka<sup>125</sup>, H. Hayashii<sup>126</sup>, S. Hazra<sup>127</sup>, M. T. Hedges<sup>128</sup>, A. Heidelberg<sup>129</sup>, I. Heredia de la Cruz<sup>130</sup>, M. Hernández Villanueva<sup>131</sup>, T. Higuchi<sup>132</sup>, M. Hoek<sup>133</sup>, M. Hohmann<sup>134</sup>, R. Hoppe<sup>135</sup>, P. Horak<sup>136</sup>, C.-L. Hsu<sup>137</sup>, T. Humair<sup>138</sup>, T. Iijima<sup>139</sup>, K. Inami<sup>140</sup>, N. Ipsita<sup>141</sup>, A. Ishikawa<sup>142</sup>, R. Itoh<sup>143</sup>, M. Iwasaki<sup>144</sup>, D. Jacobi<sup>145</sup>, W. W. Jacobs<sup>146</sup>, E.-J. Jang<sup>147</sup>, Y. Jin<sup>148</sup>, A. Johnson<sup>149</sup>, H. Junkerkalefeld<sup>150</sup>, D. Kalita<sup>151</sup>, A. B. Kaliyar<sup>152</sup>, J. Kandra<sup>153</sup>, G. Karyan<sup>154</sup>, T. Kawasaki<sup>155</sup>, F. Keil<sup>156</sup>, C. Ketter<sup>157</sup>, C. Kiesling<sup>158</sup>, C.-H. Kim<sup>159</sup>, D. Y. Kim<sup>160</sup>, J.-Y. Kim<sup>161</sup>, K.-H. Kim<sup>162</sup>, Y.-K. Kim<sup>163</sup>, K. Kinoshita<sup>164</sup>, P. Kodyš<sup>165</sup>, T. Koga<sup>166</sup>, S. Kohani<sup>167</sup>, K. Kojima<sup>168</sup>, A. Korobov<sup>169</sup>, S. Korpar<sup>170</sup>, E. Kovalenko<sup>171</sup>, R. Kowalewski<sup>172</sup>, P. Križan<sup>173</sup>, P. Krokovny<sup>174</sup>, T. Kuhr<sup>175</sup>, Y. Kullii<sup>176</sup>, R. Kumar<sup>177</sup>, K. Kumara<sup>178</sup>, T. Kunigo<sup>179</sup>, A. Kuzmin<sup>180</sup>, Y.-J. Kwon<sup>181</sup>, S. Lacaparra<sup>182</sup>, K. Lalwani<sup>183</sup>, T. Lam<sup>184</sup>, L. Lancieri<sup>185</sup>, J. S. Lange<sup>186</sup>, T. S. Lau<sup>187</sup>, M. Laurenza<sup>188</sup>, R. Lebourier<sup>189</sup>, F. R. Le Diberder<sup>190</sup>, M. J. Lee<sup>191</sup>, C. Lemettais<sup>192</sup>, P. Leo<sup>193</sup>, L. K. Li<sup>194</sup>, Q. M. Li<sup>195</sup>, W. Z. Li<sup>196</sup>, Y. Li<sup>197</sup>, Y. B. Li<sup>198</sup>, Y. P. Liao<sup>199</sup>, J. Libby<sup>200</sup>, J. Lin<sup>201</sup>, S. Lin<sup>202</sup>, M. H. Liu<sup>203</sup>, Q. Y. Liu<sup>204</sup>, Z. Q. Liu<sup>205</sup>, D. Liventsev<sup>206</sup>, S. Longo<sup>207</sup>, T. Lueck<sup>208</sup>, T. Luo<sup>209</sup>, C. Lyu<sup>210</sup>, Y. Ma<sup>211</sup>, C. Madaan<sup>212</sup>, M. Maggiora<sup>213</sup>, S. P. Maharana<sup>214</sup>, R. Maiti<sup>215</sup>, G. Mancinelli<sup>216</sup>, R. Manfredi<sup>217</sup>, E. Manoni<sup>218</sup>, M. Mantovano<sup>219</sup>, D. Marcantonio<sup>220</sup>, S. Marcello<sup>221</sup>, C. Marinas<sup>222</sup>, C. Martellini<sup>223</sup>, A. Martens<sup>224</sup>, A. Martini<sup>225</sup>, T. Martinov<sup>226</sup>, L. Massaccesi<sup>227</sup>, M. Masuda<sup>228</sup>, K. Matsuoka<sup>229</sup>, D. Matvienko<sup>230</sup>, S. K. Maurya<sup>231</sup>, M. Maushart<sup>232</sup>, J. A. McKenna<sup>233</sup>, F. Meier<sup>234</sup>, D. Meleshko<sup>235</sup>, M. Merola<sup>236</sup>, C. Miller<sup>237</sup>, M. Mirra<sup>238</sup>, S. Mitra<sup>239</sup>, K. Miyabayashi<sup>240</sup>, H. Miyake<sup>241</sup>, G. B. Mohanty<sup>242</sup>, S. Mondal<sup>243</sup>, S. Moneta<sup>244</sup>, H.-G. Moser<sup>245</sup>, R. Mussa<sup>246</sup>, I. Nakamura<sup>247</sup>, M. Nakao<sup>248</sup>, H. Nakazawa<sup>249</sup>, Y. Nakazawa<sup>250</sup>, M. Naruki<sup>251</sup>, Z. Natkaniec<sup>252</sup>, A. Natochii<sup>253</sup>, M. Nayak<sup>254</sup>, G. Nazaryan<sup>255</sup>, M. Neu<sup>256</sup>, S. Nishida<sup>257</sup>, S. Ogawa<sup>258</sup>, H. Ono<sup>259</sup>, Y. Onuki<sup>260</sup>, G. Pakhlova<sup>261</sup>, S. Pardi<sup>262</sup>, H. Park<sup>263</sup>, J. Park<sup>264</sup>, K. Park<sup>265</sup>, S.-H. Park<sup>266</sup>, A. Passeri<sup>267</sup>, S. Patra<sup>268</sup>, T. K. Pedlar<sup>269</sup>, I. Peruzzi<sup>270</sup>, R. Peschke<sup>271</sup>, R. Pestotnik<sup>272</sup>, L. E. Piilonen<sup>273</sup>, P. L. M. Podesta-Lerma<sup>274</sup>, T. Podobnik<sup>275</sup>, S. Pokharel<sup>276</sup>, C. Praz<sup>277</sup>, S. Prell<sup>278</sup>, E. Prencipe<sup>279</sup>, M. T. Prim<sup>280</sup>, I. Prudnikov<sup>281</sup>, H. Purwar<sup>282</sup>, S. Raiz<sup>283</sup>, K. Ravindran<sup>284</sup>, J. U. Rehman<sup>285</sup>, M. Reif<sup>286</sup>, S. Reiter<sup>287</sup>, M. Remnev<sup>288</sup>, L. Reuter<sup>289</sup>, D. Ricalde Herrmann<sup>290</sup>, I. Ripp-Baudot<sup>291</sup>, G. Rizzo<sup>292</sup>, M. Roehrken<sup>293</sup>, J. M. Roney<sup>294</sup>, A. Rostomyan<sup>295</sup>, D. A. Sanders<sup>296</sup>, S. Sandilya<sup>297</sup>, L. Santelj<sup>298</sup>, V. Savinov<sup>299</sup>, B. Scavino<sup>300</sup>, C. Schwanda<sup>301</sup>, A. J. Schwartz<sup>302</sup>, Y. Seino<sup>303</sup>, A. Selce<sup>304</sup>, K. Senyo<sup>305</sup>, J. Serrano<sup>306</sup>, M. E. Sevir<sup>307</sup>, C. Sfienti<sup>308</sup>, W. Shan<sup>309</sup>, X. D. Shi<sup>310</sup>, T. Shillington<sup>311</sup>, T. Shimasaki<sup>312</sup>, J.-G. Shiu<sup>313</sup>, D. Shtol<sup>314</sup>, B. Shwartz<sup>315</sup>, A. Sibidanov<sup>316</sup>, F. Simon<sup>317</sup>, J. Skorupa<sup>318</sup>, R. J. Sobie<sup>319</sup>, M. Sobotzik<sup>320</sup>, A. Soffer<sup>321</sup>, A. Sokolov<sup>322</sup>, E. Solovieva<sup>323</sup>, S. Spataro<sup>324</sup>, B. Spruck<sup>325</sup>, W. Song<sup>326</sup>, M. Starič<sup>327</sup>, P. Stavroulakis<sup>328</sup>, S. Stefkova<sup>329</sup>, R. Stroili<sup>330</sup>, J. Strube<sup>331</sup>, M. Sumihama<sup>332</sup>, K. Sumisawa<sup>333</sup>, N. Suwonjandee<sup>334</sup>, H. Svidras<sup>335</sup>, M. Takizawa<sup>336</sup>, U. Tamponi<sup>337</sup>, K. Tanida<sup>338</sup>, F. Tenchini<sup>339</sup>, A. Thaller<sup>340</sup>, O. Tittel<sup>341</sup>, R. Tiwary<sup>342</sup>, E. Torassa<sup>343</sup>, K. Trabelsi<sup>344</sup>, I. Tsaklidis<sup>345</sup>, I. Ueda<sup>346</sup>, T. Uglov<sup>347</sup>, K. Unger<sup>348</sup>, Y. Unno<sup>349</sup>, K. Uno<sup>350</sup>, S. Uno<sup>351</sup>, P. Urquijo<sup>352</sup>, Y. Ushiroda<sup>353</sup>, S. E. Vahsen<sup>354</sup>, R. van Tonder<sup>355</sup>, K. E. Varvell<sup>356</sup>, M. Veronesi<sup>357</sup>, A. Vinokurova<sup>358</sup>, V. S. Vismaya<sup>359</sup>, L. Vitale<sup>360</sup>, V. Vobbilisetti<sup>361</sup>, R. Volpe<sup>362</sup>, M. Wakai<sup>363</sup>, S. Wallner<sup>364</sup>, M.-Z. Wang<sup>365</sup>, A. Warburton<sup>366</sup>, M. Watanabe<sup>367</sup>, S. Watanuki<sup>368</sup>, C. Wessel<sup>369</sup>, E. Won<sup>370</sup>, X. P. Xu<sup>371</sup>, B. D. Yabsley<sup>372</sup>, S. Yamada<sup>373</sup>, W. Yan<sup>374</sup>, J. Yelton<sup>375</sup>, K. Yoshihara<sup>376</sup>, C. Z. Yuan<sup>377</sup>, J. Yuan<sup>378</sup>, Y. Yusa<sup>379</sup>, L. Zani<sup>380</sup>, V. Zhilich<sup>381</sup>, J. S. Zhou<sup>382</sup>, Q. D. Zhou<sup>383</sup>, L. Zhu<sup>384</sup>, and R. Žlebčík<sup>385</sup>

(Belle II Collaboration)

 (Received 16 December 2024; accepted 22 January 2025; published 25 February 2025)

We measure the branching fraction of the decay  $B^0 \rightarrow J/\psi\omega$  using data collected with the Belle II detector at the SuperKEKB collider. The data contain  $(387 \pm 6) \times 10^6$   $B\bar{B}$  meson pairs produced in energy-asymmetric  $e^+e^-$  collisions at the  $\Upsilon(4S)$  resonance. The measured branching fraction  $\mathcal{B}(B^0 \rightarrow J/\psi\omega) = (2.16 \pm 0.30 \pm 0.14) \times 10^{-5}$ , where the first uncertainty is statistical and the second is systematic, is more precise than previous results and constitutes the first observation of the decay with a significance of 6.5 standard deviations.

DOI: [10.1103/PhysRevD.111.032012](https://doi.org/10.1103/PhysRevD.111.032012)

## I. INTRODUCTION

Decays of  $B$  mesons into a charmonium state and a light unflavored meson are predominantly governed by color-suppressed tree diagrams involving the quark transition  $b \rightarrow c\bar{c}d$ . One such decay,  $B^0 \rightarrow J/\psi\omega$ , has not been observed yet. This mode can be used as a control channel in studies of  $B$  decays mediated by the  $b \rightarrow d\ell^+\ell^-$  transition at a  $B$  factory. Since the quark-level transition of this decay is the same as that of  $B^0 \rightarrow J/\psi\pi^0$ , its measured  $CP$  asymmetries can be used in a similar way to constrain the contributions from loop diagrams in  $B^0 \rightarrow J/\psi K^0$ , as in Refs. [1,2].

The LHCb experiment reported the first evidence for  $B^0 \rightarrow J/\psi\omega$  by reconstructing the mode  $\omega \rightarrow \pi^+\pi^-\pi^0$  [3]. They found a significance of 4.6 standard deviations ( $\sigma$ ) using the negative log likelihood scan and taking into account systematic uncertainties related to the fit function. Furthermore, LHCb studied the resonant structure of the decay  $B^0 \rightarrow J/\psi\pi^+\pi^-$  using an amplitude analysis and found the branching fraction to be  $\mathcal{B}(B^0 \rightarrow J/\psi\omega) = (1.8_{-0.5}^{+0.7}) \times 10^{-5}$  with the  $\omega$  decaying to  $\pi^+\pi^-$  [4].

We present a measurement of the branching fraction of the decay  $B^0 \rightarrow J/\psi\omega$  using a sample of energy-asymmetric  $e^+e^-$  collisions at the  $\Upsilon(4S)$  resonance provided by the SuperKEKB accelerator [5] and collected with the Belle II detector [6]. This sample has an integrated luminosity of  $(365.4 \pm 1.7) \text{ fb}^{-1}$  and contains  $(387 \pm 6) \times 10^6$   $B\bar{B}$  events [7]. We also use an off-resonance sample totaling  $(42.7 \pm 0.2) \text{ fb}^{-1}$  recorded 60 MeV below the  $\Upsilon(4S)$  resonance to study the background from the continuum  $e^+e^- \rightarrow q\bar{q}$  events, where  $q$  denotes a  $u$ ,  $d$ ,  $s$ , or  $c$  quark.

We reconstruct  $B^0$  mesons in the  $J/\psi\omega$  final state using the subdecays  $J/\psi \rightarrow \ell^+\ell^-$  (with  $\ell$  being an electron or a muon),  $\omega \rightarrow \pi^+\pi^-\pi^0$ , and  $\pi^0 \rightarrow \gamma\gamma$ . We extract the signal

yields by fitting distributions of signal candidates in a kinematic observable that discriminates against backgrounds. We validate our analysis procedure on simulated samples and correct for differences between collision data and simulation using control samples. Charge-conjugated modes are included throughout the paper unless explicitly stated.

## II. EXPERIMENT

The Belle II detector operates at the SuperKEKB accelerator at KEK, which collides 7 GeV electrons with 4 GeV positrons. The detector is designed to reconstruct the decay products of heavy-flavor hadrons and  $\tau$  leptons. It consists of several subsystems arranged cylindrically around the interaction point (IP). The innermost part of the detector is equipped with a two-layer silicon-pixel detector (PXD), surrounded by a four-layer double-sided silicon-strip detector (SVD) [8]. Together, they provide information about charged-particle trajectories (tracks) and decay-vertex positions. Of the outer PXD layer, only one-sixth is installed for the data used in this work. The momenta and electric charges of charged particles are determined with a 56-layer central drift chamber (CDC). Charged-particle identification (PID) is provided by a time-of-propagation counter and an aerogel ring-imaging Cherenkov counter, located outside the CDC in the barrel and forward regions, respectively. The CDC provides additional PID information through the measurement of specific ionization. Photons are identified and electrons are reconstructed by an electromagnetic calorimeter (ECL) made of CsI(Tl) crystals, covering the region outside of the PID detectors. The tracking and PID subsystems, and the calorimeter, are surrounded by a superconducting solenoid, providing an axial magnetic field of 1.5 T. The central axis of the solenoid defines the  $z$  axis of the laboratory frame, pointing approximately in the direction of the electron beam. Outside of the magnet lies the muon and  $K_L^0$  identification system, which consists of iron plates interspersed with resistive-plate chambers and plastic scintillators.

We use Monte Carlo (MC) simulated events to model signal and background distributions, study the detector

*Published by the American Physical Society under the terms of the Creative Commons Attribution 4.0 International license. Further distribution of this work must maintain attribution to the author(s) and the published article's title, journal citation, and DOI. Funded by SCOAP<sup>3</sup>.*

response, and test the analysis procedure. Quark-antiquark pairs from  $e^+e^-$  collisions are generated using KKMC [9] with Pythia8 [10]. Signal and other  $B$ -meson decays are generated with EvtGen [11]. Effects of final-state radiation are incorporated with Photos [12]. The detector response is simulated with Geant4 [13]. We use a simulated sample of generic  $e^+e^-$  collisions, corresponding to an integrated luminosity of approximately four times that of the experimental dataset. We also use large samples of simulated  $B\bar{B}$  pairs in which one of the  $B$  mesons is forced to decay to the final state of interest, while the other  $B$  meson in the event decays inclusively. One sample is used to study the signal, where the  $B$  meson decays as  $B^0 \rightarrow J/\psi\omega$ . The other samples are used to study the dominant source of background, where the  $B$  meson decays inclusively into  $B \rightarrow J/\psi X$  modes. We process collision data and simulated samples using the Belle II analysis software [14,15].

### III. EVENT SELECTION

Events containing a  $B\bar{B}$  pair are selected by a hardware trigger system based on the track multiplicity and total energy deposited in the ECL. The trigger efficiency is close to 100% for signal decays.

We reconstruct  $B^0 \rightarrow J/\psi\omega$  candidates using the decay chain  $J/\psi \rightarrow \ell^+\ell^-$ ,  $\omega \rightarrow \pi^+\pi^-\pi^0$ , and  $\pi^0 \rightarrow \gamma\gamma$ . Tracks are reconstructed using information from the PXD, SVD, and CDC [16]. Each track must have a polar angle  $\theta$  within the CDC acceptance ( $17^\circ < \theta < 150^\circ$ ) and is also required to have a distance of closest approach to the IP less than 2.0 cm along the  $z$  axis and less than 0.5 cm in the transverse plane to reduce contamination from misreconstructed and beam background-induced tracks. Electron identification is provided by a boosted decision tree (BDT) classifier that combines several ECL variables and PID likelihoods [17]. Muons are identified with the discriminator  $\mathcal{P}_\mu = \mathcal{L}_\mu / (\mathcal{L}_e + \mathcal{L}_\mu + \mathcal{L}_\pi + \mathcal{L}_K + \mathcal{L}_d + \mathcal{L}_p)$ , where the likelihood  $\mathcal{L}_i$  for each charged-particle hypothesis combines PID information from all subdetectors except for the SVD and PXD. We classify tracks as electrons or muons based on a PID requirement that is 91.1% (88.2%) efficient on signal while rejecting 99.6% (95.1%) of tracks for electrons (muons). The momenta of electrons are corrected for energy loss due to bremsstrahlung by adding the four-momenta of photons detected within 50 mrad of the initial direction of the electron tracks. Charged pions are selected by requiring the pion likelihood ratio  $\mathcal{L}_\pi / (\mathcal{L}_\pi + \mathcal{L}_K)$  to be greater than a certain threshold, which retains 98.1% of signal pions while rejecting 92.8% of kaons.

The  $J/\psi$  candidates are formed by combining oppositely charged lepton pairs having an invariant mass  $m(e^+e^-) \in [2.95, 3.15]$  GeV/ $c^2$  and  $m(\mu^+\mu^-) \in [3.0, 3.15]$  GeV/ $c^2$ , where the average  $J/\psi$  invariant mass resolution is 16(13) MeV/ $c^2$  in the  $e^+e^-$  ( $\mu^+\mu^-$ ) mode.

Photons are identified from ECL energy deposits greater than 80, 40, and 30 MeV in the forward, backward and barrel regions, respectively. The corresponding polar-angle coverages are  $[12.4, 31.4]^\circ$ ,  $[130.7, 155.1]^\circ$ , and  $[32.2, 128.7]^\circ$ . The ECL energy deposits are required to have no matched tracks in the CDC. Photon energy corrections are derived from an  $e^+e^- \rightarrow \mu^+\mu^-\gamma$  control sample reconstructed in data. The  $\pi^0$  candidates are formed by combining pairs of photons with an invariant mass  $m(\gamma\gamma) \in [0.120, 0.145]$  GeV/ $c^2$ . The average  $\pi^0$  invariant mass resolution is 8 MeV/ $c^2$ .

The  $\omega$  candidates are formed by combining  $\pi^0$  candidates with two oppositely charged pions with an invariant mass  $m(\pi^+\pi^-\pi^0) \in [0.73, 0.83]$  GeV/ $c^2$ . The average  $\omega$  invariant mass resolution is 15 MeV/ $c^2$ .

The  $B^0 \rightarrow J/\psi\omega$  decay vertex is determined using the TreeFitter algorithm [18,19]. The  $J/\psi$  invariant mass is constrained to its known value [20]. We retain  $B$  candidates with a successful vertex fit. The beam-energy constrained mass  $M_{bc}$  and energy difference  $\Delta E$  are computed for each  $B^0 \rightarrow J/\psi\omega$  candidate as  $M_{bc} \equiv \sqrt{(E_{beam}^*/c^2)^2 - (|p_B^*/c|^2)}$  and  $\Delta E \equiv E_B^* - E_{beam}^*$ , where  $E_{beam}^*$  is the beam energy, and  $E_B^*$  and  $p_B^*$  are the energy and momentum of the  $B^0$  candidate, respectively, all calculated in the center-of-mass (c.m.) frame. Signal  $B^0$  candidates peak at the known  $B^0$  mass [20] in  $M_{bc}$  and zero in  $\Delta E$ . The average  $M_{bc}$  and  $\Delta E$  resolutions for correctly reconstructed signal events are 3 MeV/ $c^2$  and 20 MeV, respectively. Candidates satisfying  $M_{bc} > 5.27$  GeV/ $c^2$  and  $|\Delta E| < 0.25$  GeV are retained for further analysis.

We suppress the contribution from the dominant source of background  $B \rightarrow J/\psi X$  decays that do not contain a true  $\omega$  meson, using BDT classifiers [21] that combine several variables to discriminate between signal and background. We use a separate BDT for each  $J/\psi$  decay mode because the background shapes are mode dependent. The BDTs are trained on the following six input variables: the momentum of the  $\pi^0$  candidate in the laboratory frame, the invariant mass of the  $\omega$  candidate, the invariant masses of the  $\pi^0\pi^+$  and  $\pi^0\pi^-$  systems, and the invariant masses of the  $\pi^+\pi^-$  system, calculated by assigning a kaon mass hypothesis to the positively (negatively) charged pion while retaining a pion mass hypothesis for the negatively (positively) charged pion.

To validate the MC modeling of BDT input variables, we compare their distributions in the  $M_{bc}$  and  $\Delta E$  sidebands in simulation and data and find them to agree well. The  $M_{bc}$  sidebands correspond to the region  $5.20 < M_{bc} < 5.25$  GeV/ $c^2$ , which excludes 100% of the simulated signal. The  $\Delta E$  sidebands are chosen so that the central 99.97% of the simulated signal is excluded:  $\Delta E \in [-0.250, -0.148] \cup [0.102, 0.250]$  GeV in the  $e^+e^-$  mode and  $[-0.250, -0.147] \cup [0.094, 0.250]$  GeV in the  $\mu^+\mu^-$  mode. We train the BDTs using signal and background



samples from simulated data. For each BDT, we choose a criterion to be applied on its output by optimizing a figure of merit  $S/\sqrt{S+B}$ , where  $S$  and  $B$  are the number of correctly reconstructed signal and background candidates in the  $\Delta E$  region containing the central 95% of the signal. In the calculation of the figure of merit we use the current world-average values of the signal and  $B^0 \rightarrow J/\psi X$  branching fractions [20]. The BDT selection retains 62.0% (59.1%) of the signal while rejecting 90.1% (91.3%) of the background in the  $e^+e^-$  ( $\mu^+\mu^-$ ) mode.

Events with more than one candidate account for approximately 9% of the events selected in the collision data. For events with multiple candidates, we retain the one with the highest BDT score. This requirement selects the correct signal candidate 68% of the time for events with multiple candidates in simulation.

To account for data-MC differences in the signal probability density function, we reconstruct a control mode with the same final state,  $B^0 \rightarrow J/\psi K^{*0}$ , with  $K^* \rightarrow K_S^0 \pi^0$ ,  $K_S^0 \rightarrow \pi^+ \pi^-$ , and  $\pi^0 \rightarrow \gamma\gamma$ . We apply the same event selection, except for the requirements on the pion tracks from the  $K_S^0$ , since the  $K_S^0$  reconstruction is cleaner than the  $\omega$  reconstruction. We also use a different  $m(\pi^+ \pi^- \pi^0)$  requirement. The  $K_S^0$  candidates are formed by combining oppositely charged tracks and requiring  $m(\pi^+ \pi^-) \in [0.45, 0.55]$  GeV/ $c^2$ . The  $K^{*0}$  candidates are required to have an invariant mass  $m(\pi^+ \pi^- \pi^0) \in [0.817, 0.967]$  GeV/ $c^2$ . We also require the cosine of the angle between the  $B^0$  and  $\pi^0$  momenta in the  $K^{*0}$  rest frame to be greater than  $-0.7$ .

To account for data-MC differences in the efficiency of the  $J/\psi$  vertex fit, we reconstruct an inclusive  $J/\psi$  control mode by applying the same  $J/\psi$  selection as in the signal mode.

To validate the BDT, we reconstruct another control mode,  $D^0 \rightarrow K_S^0 \omega$ , with  $\omega \rightarrow \pi^+ \pi^- \pi^0$  and  $K_S^0 \rightarrow \pi^+ \pi^-$ . Since the BDT input variables depend only on the decay products of the  $\omega$ , and all but the laboratory-frame  $\pi^0$  momentum are Lorentz invariant, we choose a control mode that has high  $\omega$  purity in order to calibrate the signal efficiency of the BDT selection. We apply the same  $\omega$  selection as in the signal mode and the same  $K_S^0$  selection as in the  $B^0 \rightarrow J/\psi K^{*0}$  control mode. The  $D^0$  candidate is formed by combining the  $\omega$  and  $K_S^0$  using the TreeFitter algorithm [18,19]. We require the  $\chi^2$  probability of the  $D^0$  vertex fit to be greater than 0.1%. A  $D^{*+}$  candidate is formed by combining a track with a pion mass hypothesis and the  $D^0$  candidate. We suppress background from  $B\bar{B}$  decays by requiring the momentum of the  $D^{*+}$  candidates in the  $\Upsilon(4S)$  c.m. frame to be greater than 2.4 GeV/ $c$ . We further require that the mass difference between the  $D^{*+}$  and  $D^0$  candidates be in the range  $[0.1445, 0.1465]$  GeV/ $c^2$ . The BDT input variables' distributions in reconstructed  $D^0 \rightarrow K_S^0 \omega$  decays show good agreement between data and simulation.

TABLE I. Signal efficiencies corrected for data-MC differences (uncertainties are systematic), signal yields corrected for non-resonant contribution and background yields (uncertainties are statistical), as well as statistical significances.

Decay mode	$\epsilon_{\text{sig}}$ [%]	$n'_{\text{sig}}$	$n_{\text{bkg}}$	Stat. Sig. [ $\sigma$ ]
$J/\psi \rightarrow e^+e^-$	$13.7 \pm 0.7$	$54 \pm 11$	$206 \pm 16$	4.9
$J/\psi \rightarrow \mu^+\mu^-$	$13.2 \pm 0.7$	$61 \pm 12$	$210 \pm 17$	5.2

The signal efficiencies corrected for differences between data and simulation are listed in Table I.

#### IV. SIGNAL EXTRACTION FIT

The sample passing the event selection is populated by  $B^0 \rightarrow J/\psi \omega$  candidates coming from both signal and backgrounds. For signal events with multiple candidates, simulation studies show that incorrectly selected signal candidates, based on their BDT scores, are predominantly due to misreconstructed  $\omega$  mesons with a low-momentum  $\pi^0 \rightarrow \gamma\gamma$  originating from the other  $B$  meson decay. The  $\Delta E$  distribution of these incorrectly selected  $B^0$  candidates is centered around zero and resembles the distribution of correctly reconstructed signal candidates. Consequently, they are also treated as signal candidates in the measurement.

Among various sources of background, the largest contribution comes from  $B \rightarrow J/\psi X$  decays, for which the  $J/\psi$  is correctly reconstructed but originates from a different  $B$  decay than the signal. There is also a contribution from  $B\bar{B}$  events with misreconstructed  $J/\psi$  and continuum backgrounds, which accounts for 4% (15%) of candidates in the  $e^+e^-$  ( $\mu^+\mu^-$ ) mode in simulation. The  $\mu^+\mu^-$  mode has a higher background here since the muon PID requirement has a higher fake rate than that of the electron. We validate our suppression of continuum background by applying the selection criteria to the off-resonance sample. We find a background yield consistent with our expectation from simulation.

The selection efficiency in simulation for nonresonant  $B^0 \rightarrow J/\psi \pi^+ \pi^- \pi^0$  decays generated with a phase space model is less than 1% of our signal selection efficiency. The branching fraction of these nonresonant decays has not been measured. From a fit to the  $\Delta E$  distribution in the  $\omega$  invariant mass sidebands,  $m(\pi^+ \pi^- \pi^0) \in [0.60, 0.73] \cup [0.83, 1.00]$  GeV/ $c^2$ , we expect a contribution from non-resonant decays of  $1.9 \pm 3.0$  ( $3.6 \pm 3.1$ ) in the  $\omega$  invariant mass signal window in the  $e^+e^-$  ( $\mu^+\mu^-$ ) mode. We correct the fitted signal yields by the central values and take the statistical uncertainties as a systematic uncertainty. The interference between the signal and nonresonant decays is calculated assuming the latter branching fraction to be the same as that of the signal and its impact on the signal yields is found to be negligible.

We extract the signal yields from an extended maximum-likelihood fit to the unbinned  $\Delta E$  distributions. The

probability density function (PDF) of the signal is described by a double-sided Crystal Ball ( $F_{\text{CB}}$ ) function [22,23] with all parameters excluding the mean  $\mu$  determined from simulation:  $\sigma$ ,  $\alpha_L$ ,  $n_L$ ,  $\alpha_R$ , and  $n_R$ . We account for the data-MC differences by scaling the width  $\sigma$  of the Gaussian core of  $F_{\text{CB}}$  with a scale factor obtained by fitting the  $B^0 \rightarrow J/\psi K^{*0}$  control sample. The difference in  $\Delta E$  shape between the two  $J/\psi$  decay modes is negligible. Therefore, the parameters of the signal PDF are shared between  $J/\psi \rightarrow e^+e^-$  and  $J/\psi \rightarrow \mu^+\mu^-$  modes. Each background component has a smooth  $\Delta E$  distribution, enabling us to model the distribution of the sum of all backgrounds using an exponential PDF ( $F_{\text{exp}}$ ).

In the fit to the data, we determine the signal and background yields,  $n_{\text{sig}}$  and  $n_{\text{bkg}}$ , separately for the  $J/\psi \rightarrow e^+e^-$  and  $J/\psi \rightarrow \mu^+\mu^-$  modes, the mean  $\mu$  of the signal PDF, and the exponential decay parameters of the background PDF,  $c^i$ . In total, the fit has seven free and five fixed parameters. The likelihood function is

$$\mathcal{L} = \frac{e^{-(n_{\text{sig}}+n_{\text{bkg}})}}{N!} \prod_{i=1}^N \{n_{\text{sig}} F_{\text{CB}}^i + n_{\text{bkg}} F_{\text{exp}}^i\} \quad (1)$$

where  $i$  is the index of the candidate,  $N$  is the total number of candidates in the dataset, and  $F_{\text{CB}}^i$  and  $F_{\text{exp}}^i$  are the signal and background PDFs of the  $i$ th candidate, respectively. In total, we fit 262 (274) candidates in the  $e^+e^-$  ( $\mu^+\mu^-$ ) mode. The data and the fit are shown in Fig. 1. Table I lists the signal selection efficiencies, fitted yields of signal (corrected for nonresonant contribution) and background, as well as the statistical significances that are calculated by dividing the central values by the statistical errors.

From the signal yields, we determine the branching fraction:

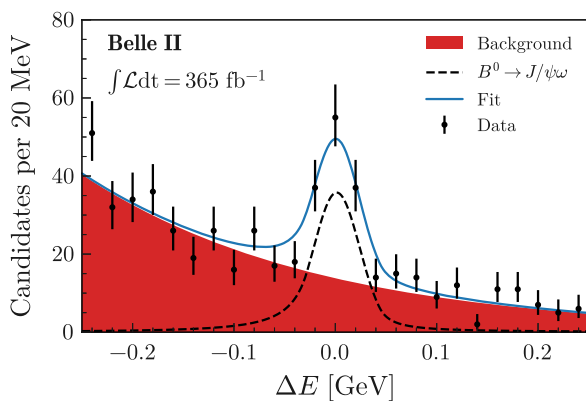


FIG. 1. Distribution of  $\Delta E$  for  $B^0 \rightarrow J/\psi\omega$  candidates (data points) with fit overlaid (curves and filled area). The background component includes contributions from  $B^0 \rightarrow J/\psi X$ , other  $B\bar{B}$  decays, and continuum events.

$$\mathcal{B} = \frac{(n_{\text{sig}}^{e^+e^-}/\epsilon_{\text{sig}}^{e^+e^-} + n_{\text{sig}}^{\mu^+\mu^-}/\epsilon_{\text{sig}}^{\mu^+\mu^-})(1 + f_{+-}/f_{00})}{\mathcal{B}(J/\psi \rightarrow \ell^+\ell^-)\mathcal{B}(\omega \rightarrow \pi^+\pi^-\pi^0)\mathcal{B}(\pi^0 \rightarrow \gamma\gamma)2N_{B\bar{B}}} \quad (2)$$

where  $\epsilon_{\text{sig}}$  are the efficiencies obtained from simulated signal samples and corrected for data-MC differences using control samples,  $\mathcal{B}(J/\psi \rightarrow \ell^+\ell^-)$  is the sum of  $\mathcal{B}(J/\psi \rightarrow e^+e^-) = (5.971 \pm 0.032)\%$  and  $\mathcal{B}(J/\psi \rightarrow \mu^+\mu^-) = (5.961 \pm 0.033)\%$ ,  $\mathcal{B}(\omega \rightarrow \pi^+\pi^-\pi^0)$  is  $(89.2 \pm 0.7)\%$ ,  $\mathcal{B}(\pi^0 \rightarrow \gamma\gamma)$  is  $(98.823 \pm 0.034)\%$  [20],  $N_{B\bar{B}} = (387 \pm 6) \times 10^6$  is the number of  $B\bar{B}$  pairs in the dataset, and  $f_{+-}/f_{00} = 1.052 \pm 0.031$  [24] is the ratio of branching fractions for the  $\Upsilon(4S)$  decays to  $B^+B^-$  and  $B^0\bar{B}^0$ . We obtain  $\mathcal{B}(B^0 \rightarrow J/\psi\omega) = (2.16 \pm 0.30) \times 10^{-5}$ , where the uncertainty is statistical only.

## V. SYSTEMATIC UNCERTAINTIES

Table II lists contributions from various sources of systematic uncertainty. Below, we describe each of them as well as the procedure to estimate their contributions.

In the calculation of the branching fraction, we correct the signal efficiencies obtained in simulation using control samples in the data. The statistical and systematic uncertainties associated with the correction factors are propagated together as a systematic uncertainty on the measured branching fraction.

Tracking efficiencies are measured with  $e^+e^- \rightarrow \tau^+\tau^-$  events, where one  $\tau$  decays as  $\tau^- \rightarrow e^-\bar{\nu}_e\nu_\tau$  and the other as  $\tau^- \rightarrow \pi^-\pi^+\pi^-\nu_\tau$ . A difference of 0.27% for each track is observed between data and simulation, which is propagated to the uncertainty on the branching fraction.

TABLE II. Relative systematic uncertainties on the branching fraction  $\mathcal{B}(B^0 \rightarrow J/\psi\omega)$  compared with the statistical uncertainty.

Source	Relative uncertainty [%]
Tracking efficiency	1.1
$\pi^0$ reconstruction	3.8
Lepton identification	+0.7 -0.5
$J/\psi$ vertex fit	0.2
$\omega$ vertex fit	1.2
$\omega$ mass window	1.5
BDT selection	1.2
Longitudinal polarization fraction	+1.1 -1.0
Signal model	0.6
Fixed PDF parameters	3.0
Nonresonant background	2.1
Background model	1.4
External inputs	0.9
$N_{B\bar{B}}$	1.5
$f_{+-}/f_{00}$	1.5
Total systematic uncertainty	6.6
Statistical uncertainty	14.0

The  $\pi^0$  reconstruction efficiency is measured in data and simulation from the ratio of the yields of  $D^{*+} \rightarrow D^0(\rightarrow K^-\pi^+\pi^0)\pi^+$  and  $D^{*+} \rightarrow D^0(\rightarrow K^-\pi^+)\pi^+$ , scaled by the inverse of their branching fractions. The yield ratio in collision and simulated data is used to obtain correction factors as a function of the  $\pi^0$  momentum and polar angle. The average correction factor of the  $\pi^0$  efficiency in  $B^0 \rightarrow J/\psi\omega$  decays is  $0.99 \pm 0.04$ , with the uncertainty dominated by the knowledge of the  $D^0$ -decay branching fractions [20].

The data-MC difference in electron and muon identification performance is calibrated with  $J/\psi \rightarrow \ell^+\ell^-$ ,  $e^+e^- \rightarrow \ell^+\ell^-(\gamma)$ , and  $e^+e^- \rightarrow e^+e^-\ell^+\ell^-$  samples. The average correction factor over the kinematic distribution of the signal is  $0.991 \pm 0.009$  ( $0.924 \pm 0.010$ ) for the  $e^+e^-(\mu^+\mu^-)$  mode, where the uncertainties are calculated as the quadrature sum of the statistical and systematic uncertainties.

The difference in pion identification performance between simulation and data is calibrated with samples of  $D^0 \rightarrow K^-\pi^+$  and  $K_S^0 \rightarrow \pi^+\pi^-$  decays. The uncertainty on the average correction factor over the kinematic distribution of the signal is negligible.

The vertex fit efficiencies for the  $J/\psi$  and  $\omega$  are determined by calculating the ratio of signal yields with and without the vertex constraint for both collision and simulated events using inclusive  $J/\psi$  and  $D^0 \rightarrow K_S^0\omega$  control samples. We fit the invariant mass distributions of the selected  $J/\psi$  and  $\omega$  candidates from the control samples to extract the signal yields. The measured efficiencies in data and simulation are consistent within statistical uncertainties. The statistical uncertainties on the data-MC ratio of efficiencies are assigned as the systematic uncertainties due to vertex fit constraints. Additionally, we measure the efficiency of the  $\omega$  invariant mass window by fitting the corresponding distribution from the  $D^0 \rightarrow K_S^0\omega$  control sample. The efficiencies obtained in data and simulation are statistically consistent, and the statistical uncertainty on their ratio is taken as the systematic uncertainty associated with the  $\omega$  invariant mass window selection.

The performance of the fake  $\omega$  suppression BDT is validated with the control mode  $D^0 \rightarrow K_S^0\omega$ . The ratio of the signal efficiency in data and simulation due to the BDT requirement is  $0.99 \pm 0.01$  ( $0.99 \pm 0.02$ ) in the  $e^+e^-(\mu^+\mu^-)$  mode, where the uncertainty is statistical only. The uncertainty, including the correlation between corrections for the two  $J/\psi$  decay modes, is propagated to the uncertainty on the branching fraction.

The signal efficiency depends on the longitudinal polarization fraction of the signal decay. We simulate the signal decay with EvtGen using helicity amplitudes measured in Ref. [4]. We take the difference in the signal efficiency when varying the helicity amplitudes around their uncertainties as a systematic uncertainty.

We consider the following uncertainties associated with the signal yields obtained from the fit. We assign a systematic uncertainty due to imperfect signal modeling

using simplified simulated datasets in which the signal is sampled from simulated data and the background is generated with the exponential PDF. The systematic uncertainty is assigned to be the product of the statistical uncertainty from the fit and the mean of the distribution of the difference of the fit yield from its true value divided by the fit error. To assess the systematic uncertainty associated with fixing the width parameter in the signal PDF, we repeat the fit by varying the scale factor determined in the  $B^0 \rightarrow J/\psi K^{*0}$  control sample according to its statistical uncertainty. We take the width of the variations of fit yields from the nominal fit divided by fit errors on the signal yields and propagate it on the branching fraction. We take the statistical uncertainty on the expected nonresonant yields determined with a fit to the  $\omega$  invariant mass sidebands as a systematic uncertainty.

To test the modeling of the background exponential PDF, we perform fits using independent subsets composed of background simulated data and signal generated from the signal  $F_{CB}$  PDF. An average bias on the signal yield is obtained in the subsets. We take the uncertainty on the average bias divided by the signal yield as a systematic uncertainty due to imperfect background modeling and propagate it on the branching fraction.

We propagate the uncertainty on the branching fractions of the  $J/\psi \rightarrow \ell^+\ell^-$ ,  $\omega \rightarrow \pi^+\pi^-\pi^0$ , and  $\pi^0 \rightarrow \gamma\gamma$  subdecays used to reconstruct the signal [20]. The uncertainty on the number of  $B^0$  mesons in the sample comes from the determination of the number of  $B\bar{B}$  pairs and from the knowledge of the  $f_{+-}/f_{00}$  ratio [24].

## VI. CONCLUSION

To summarize, we have measured the branching fraction of  $B^0 \rightarrow J/\psi\omega$  decays using data from the Belle II experiment. We find  $115 \pm 16$  signal candidates in a sample of  $(387 \pm 6) \times 10^6 B\bar{B}$  events, corresponding to a decay branching fraction of

$$\mathcal{B}(B^0 \rightarrow J/\psi\omega) = (2.16 \pm 0.30 \pm 0.14) \times 10^{-5} \quad (3)$$

where the first uncertainty is statistical and the second is systematic. The total signal significance is 6.5 standard deviations, constituting the first observation of the decay. The significance is calculated by adding the statistical and systematic uncertainties in quadrature. The results are the most precise to date and consistent with earlier determinations by LHCb [3,4]. They open up the possibility of conducting a  $CP$  violation study with more data from Belle II.

## ACKNOWLEDGMENTS

This work, based on data collected using the Belle II detector, which was built and commissioned prior to March 2019, was supported by Higher Education and Science Committee of the Republic of Armenia Grant



No. 23LCG-1C011; Australian Research Council and Research Grants No. DP200101792, No. DP210101900, No. DP210102831, No. DE220100462, No. LE210100098, and No. LE230100085; Austrian Federal Ministry of Education, Science and Research, Austrian Science Fund No. P 34529, No. J 4731, No. J 4625, and No. M 3153, and Horizon 2020 ERC Starting Grant No. 947006 “InterLeptons”; Natural Sciences and Engineering Research Council of Canada, Compute Canada and CANARIE; National Key R&D Program of China under Contract No. 2022YFA1601903, National Natural Science Foundation of China and Research Grants No. 11575017, No. 11761141009, No. 11705209, No. 11975076, No. 12135005, No. 12150004, No. 12161141008, No. 12475093, and No. 12175041, and Shandong Provincial Natural Science Foundation Project No. ZR2022JQ02; the Czech Science Foundation Grant No. 22-18469S and Charles University Grant Agency Project No. 246122; European Research Council, Seventh Framework PIF-GA-2013-622527, Horizon 2020 ERC-Advanced Grants No. 267104 and No. 884719, Horizon 2020 ERC-Consolidator Grant No. 819127, Horizon 2020 Marie Skłodowska-Curie Grant Agreement No. 700525 “NIOBE” and No. 101026516, and Horizon 2020 Marie Skłodowska-Curie RISE project JENNIFER2 Grant Agreement No. 822070 (European grants); L’Institut National de Physique Nucléaire et de Physique des Particules (IN2P3) du CNRS and L’Agence Nationale de la Recherche (ANR) under grant ANR-21-CE31-0009 (France); BMBF, DFG, HGF, MPG, and AvH Foundation (Germany); Department of Atomic Energy under Project Identification No. RTI 4002, Department of Science and Technology, and UPES SEED funding programs No. UPES/R&D-SEED-INFRA/17052023/01 and No. UPES/R&D-SOE/20062022/06 (India); Israel Science Foundation Grant No. 2476/17, U.S.-Israel Binational Science Foundation Grant No. 2016113, and Israel Ministry of Science Grant No. 3-16543; Istituto Nazionale di Fisica Nucleare and the Research Grants BELLE2, and the ICSC—Centro Nazionale di Ricerca in High Performance Computing, Big Data and Quantum Computing, funded by European Union—NextGenerationEU; Japan Society for the Promotion of Science, Grant-in-Aid for Scientific Research Grants No. 16H03968, No. 16H03993, No. 16H06492, No. 16K05323, No. 17H01133, No. 17H05405, No. 18K03621, No. 18H03710, No. 18H05226, No. 19H00682, No. 20H05850, No. 20H05858, No. 22H00144, No. 22K14056, No. 22K21347, No. 23H05433, No. 26220706, and No. 26400255, and the Ministry of Education, Culture, Sports, Science, and Technology (MEXT) of Japan; National Research Foundation (NRF) of Korea Grants No. 2016R1-D1A1B-02012900, No. 2018R1-A6A1A-06024970, No. 2021R1-

A6A1A-03043957, No. 2021R1-F1A-1060423, No. 2021R1-F1A-1064008, No. 2022R1-A2C-1003993, No. 2022R1-A2C-1092335, No. RS-2023-00208693, No. RS-2024-00354342, and No. RS-2022-00197659, Radiation Science Research Institute, Foreign Large-Size Research Facility Application Supporting project, the Global Science Experimental Data Hub Center, the Korea Institute of Science and Technology Information (K24L2M1C4) and KREONET/GLORIAD; Universiti Malaya RU grant, Akademi Sains Malaysia, and Ministry of Education Malaysia; Frontiers of Science Program Contracts No. FOINS-296, No. CB-221329, No. CB-236394, No. CB-254409, and No. CB-180023, and SEP-CINVESTAV Research Grant No. 237 (Mexico); the Polish Ministry of Science and Higher Education and the National Science Center; the Ministry of Science and Higher Education of the Russian Federation and the HSE University Basic Research Program, Moscow; University of Tabuk Research Grants No. S-0256-1438 and No. S-0280-1439 (Saudi Arabia), and King Saud University, Riyadh, Researchers Supporting Project number (RSPD2024R873) (Saudi Arabia); Slovenian Research Agency and Research Grants No. J1-9124 and No. P1-0135; Agencia Estatal de Investigación, Spain Grant No. RYC2020-029875-I and Generalitat Valenciana, Spain Grant No. CIDEGENT/2018/020; The Knut and Alice Wallenberg Foundation (Sweden), Contracts No. 2021.0174 and No. 2021.0299; National Science and Technology Council, and Ministry of Education (Taiwan); Thailand Center of Excellence in Physics; TUBITAK ULAKBIM (Turkey); National Research Foundation of Ukraine, Project No. 2020.02/0257, and Ministry of Education and Science of Ukraine; the U.S. National Science Foundation and Research Grants No. PHY-1913789 and No. PHY-2111604, and the U.S. Department of Energy and Research Awards No. DE-AC06-76RLO1830, No. DE-SC0007983, No. DE-SC0009824, No. DE-SC0009973, No. DE-SC0010007, No. DE-SC0010073, No. DE-SC0010118, No. DE-SC0010504, No. DE-SC0011784, No. DE-SC0012704, No. DE-SC0019230, No. DE-SC0021274, No. DE-SC0021616, No. DE-SC0022350, No. DE-SC0023470; and the Vietnam Academy of Science and Technology (VAST) under Grants No. NVCC.05.12/22-23 and No. DL0000.02/24-25. We thank the SuperKEKB team for delivering high-luminosity collisions; the KEK cryogenics group for the efficient operation of the detector solenoid magnet and IBelle on site; the KEK Computer Research Center for on-site computing support; the NII for SINET6 network support; and the raw-data centers hosted by BNL, DESY, GridKa, IN2P3, INFN, and the University of Victoria.

These acknowledgements are not to be interpreted as an endorsement of any statement made by any of our institutes, funding agencies, governments, or their representatives.

**DATA AVAILABILITY**

The data that support the findings of this article are not publicly available. The data are available from the authors upon reasonable request.

- 
- [1] M. Ciuchini, M. Pierini, and L. Silvestrini, *Phys. Rev. Lett.* **95**, 221804 (2005).
- [2] M. Z. Barel, K. D. Bruyn, R. Fleischer, and E. Malami, *J. Phys. G* **48**, 065002 (2021).
- [3] R. Aaij *et al.* (LHCb Collaboration), *Nucl. Phys.* **B867**, 547 (2013).
- [4] R. Aaij *et al.* (LHCb Collaboration), *Phys. Rev. D* **90**, 012003 (2014).
- [5] K. Akai, K. Furukawa, and H. Koiso, *Nucl. Instrum. Methods Phys. Res., Sect. A* **907**, 188 (2018).
- [6] T. Abe *et al.* (Belle II Collaboration), arXiv:1011.0352.
- [7] I. Adachi *et al.* (Belle II Collaboration), *Chin. Phys. C* **49**, 013001 (2025).
- [8] K. Adamczyk *et al.* (Belle II SVD Group), *J. Instrum.* **17**, P11042 (2022).
- [9] S. Jadach, B. F. L. Ward, and Z. Wař, *Comput. Phys. Commun.* **130**, 260 (2000).
- [10] T. Sjöstrand, S. Ask, J. R. Christiansen, R. Corke, N. Desai, P. Ilten, S. Mrenna, S. Prestel, C. O. Rasmussen, and P. Z. Skands, *Comput. Phys. Commun.* **191**, 159 (2015).
- [11] D. J. Lange, *Nucl. Instrum. Methods Phys. Res., Sect. A* **462**, 152 (2001).
- [12] E. Barberio, B. van Eijk, and Z. Wař, *Comput. Phys. Commun.* **66**, 115 (1991).
- [13] S. Agostinelli *et al.* (GEANT4 Collaboration), *Nucl. Instrum. Methods Phys. Res., Sect. A* **506**, 250 (2003).
- [14] T. Kuhr, C. Pulvermacher, M. Ritter, T. Hauth, and N. Braun (Belle II Framework Software Group), *Comput. Software Big Sci.* **3**, 1 (2019).
- [15] 10.5281/zenodo.5574115
- [16] V. Bertacchi *et al.* (Belle II Tracking Group), *Comput. Phys. Commun.* **259**, 107610 (2021).
- [17] M. Milesi, J. Tan, and P. Urquijo, *EPJ Web Conf.* **245**, 06023 (2020).
- [18] W. D. Hulsbergen, *Nucl. Instrum. Methods Phys. Res., Sect. A* **552**, 566 (2005).
- [19] J.-F. Krohn *et al.* (Belle II Analysis Software Group), *Nucl. Instrum. Methods Phys. Res., Sect. A* **976**, 164269 (2020).
- [20] S. Navas *et al.* (Particle Data Group), *Phys. Rev. D* **110**, 030001 (2024).
- [21] T. Chen and C. Guestrin, in *Proceedings of the 22nd ACM SIGKDD International Conference on Knowledge Discovery and Data Mining, KDD '16* (Association for Computing Machinery, New York, NY, USA, 2016), pp. 785–794.
- [22] J. Gaiser, Ph.D. thesis, Stanford University, 1982.
- [23] T. Skwarnicki, Ph.D. thesis, Cracow, INP, 1986.
- [24] S. Banerjee *et al.* (HFLAV Collaboration), arXiv: 2411.18639.